Environ. Sci. Technol. **2008,** *42,* 8516–8521

Fluorination of $ZnWO_4$ Photocatalyst and Influence on the Degradation Mechanism for 4-Chlorophenol

GUANGLI HUANG,[†] SHICHENG ZHANG,[‡] TONGGUANG XU,[†] AND YONGFA ZHU*,[†]

Department of Chemistry, Tsinghua University, Beijing 100084, P. R. China, and Department of Environmental Science and Engineering, Fudan University, Shanghai 200433, P. R. China

Received June 18, 2008. Revised manuscript received July 31, 2008. Accepted September 3, 2008.

The fluorine doped $ZnWO_4$ photocatalyst was synthesized by hydrothermal synthesis and annealing treatment. The existing states of fluorine in the crystal were elucidated, and the effects of fluorine on the crystal structure, photocatalytic activity, and degradative intermediates were investigated. The doping concentration of fluorine in the interstitial lattice of $ZnWO_4$ crystal can be controlled by the annealing conditions. The photocatalytic activity can be enhanced about 50% after the doped $ZnWO_4$ was annealed at 450 °C for 1 h due to perfect crystal structure. The enhancement of photocatalytic activity after fluorine doping could be attributed to the higher separation efficiency of electron-hole pairs, which results in a large number of holes participated in the photocatalytic process. The fluorine doping does not change the degradation pathway of 4-chlorophenol (4-CP) in our system. 4-CP was mainly transformed into hydroxylated aromatic intermediates such as benzoquinone (BQ), hydroquinone (HQ), and 4-chlorocatechol (4-CC). The photodegradation of 4-CP in powdered F-doped $ZnWO_4$ system proceeded via direct holes oxidation reactions.

Introduction

In recent years, F ions acting as promising dopants in a TiO_2 and non-TiO_2 photocatalyst have attracted a great deal of attention (*1*−*3*). The photocatalysts after being doped by the F element exhibit greater enhanced photocatalytic activity than before. The interpretation of enhanced photocatalytic activities was as follows: (1) fluoride doping improves the crystallinity of anatase (*1*); (2) the doped F atoms convert Ti^{4+} to Ti^{3+} and the presence of a certain amount of Ti^{3+} reduces the electron−hole recombination rate (*2*); (3) fluorine doping results in the formation of oxygen vacancies and an increase of effective electron mobility (*3*). More recently, enhanced photocatalytic activity on $ZnWO_4$ by fluorine introduction was reported by our group (*4*). Our preliminary experiments demonstrated that the enhanced photocatalytic activities were ascribed to an increase of the transfer-rate of photogenerated electrons to the photocatalyst surface. However, further investigations to reveal details about the fluorination effect are required for a better understanding of the enhancement mechanism.

* Corresponding author phone: +86-10-62783586; fax: +86-10-62787601; e-mail: zhuyf@tsinghua.edu.cn.
[†] Tsinghua University.
[‡] Fudan University.

Chlorophenols constitute an important class of soil and water pollutants arising from their wide use as pesticides, herbicides, and wood preservatives. In particular, 4-chlorophenol (4-CP), a representative of this class, generated as a byproduct of waste incineration, can have serious consequences on human health and on the quality of the environment (*5*). The degradation of these compounds is possible via chemical, photochemical, and biological processes, but photocatalytic degradation has received considerable attention because it is environmental friendly and low cost (*6*). The photocatalytic degradation of 4-CP over Ti-based photocatalysts in aqueous solutions (*7*−*9*), in gas phase (*10*), and on film electrodes (*11*) has been investigated. These investigations have emphasized that 4-CP can be degraded either by electron attachment to the 4-CP substrate or by oxidation through attack by •OH radicals. However, there is no report on degradative mechanism and pathways of 4-CP over F-doped $ZnWO_4$ photocatalyst.

In this study, we investigated the fluorination effect on photocatalytic activity of $ZnWO_4$ and photodegradation mechanism of 4-CP. Liquid chromatography−mass spectrometry (LC-MS-MS) and diffuse reflectance infrared transmission spectra (DRS-FTIR) were exploited to understand the 4-CP photodegraded pathways. The active species during the photodegradation of 4-CP process were examined. This work may provide further understanding on the photocatalytic mechanisms for fluorine doped non-TiO_2 catalysts.

Experimental Section

Materials Preparation. Fluorine-doped $ZnWO_4$ (F-$ZnWO_4$) samples were prepared through a hydrothermal process described in the previous report (*4*). The value of R_F is used to describe the molar ratio of F to Zn, which is 0.4 nominal ratios in this study. Subsequently, different fractions were annealed for 1 h at 400 °C, 450 °C, 500 °C, 550 °C or annealed at 450 °C for 1 h, 2 h, 4 h, respectively.

Characterization. The products were characterized by powder X-ray diffraction (XRD) on a Bruker D8-advance X-ray diffractometer at 40 kV and 40 mA for monochromatized Cu Kα (λ=1.5418 Å) radiation. Morphologies of the prepared samples were further examined with transmission electron microscopy (TEM) by a JEM 1200 electron microscope operated at an accelerating voltage of 100 kV. The Brunauer−Emmett−Teller (BET) surface area was determined by ASAP 2010V5.02H. The adsorbed gas was nitrogen. The X-ray photoelectron spectroscopy (XPS) analysis was conducted on a PHI 5300 ESCA instrument using an Al Kα X-ray source at a power of 250 W. UV−vis diffuse reflectance spectrums (DRS) of the samples were measured by using Hitachi U-3010 UV−vis spectrophotometer. The concentrations of 4-CP and most of its reaction intermediates were measured by a HPLC (Agilent 1100) system. A HIQ-SU-C18 reversed phase column was employed. All substances were detected by a UV detector at 280 nm. The eluent consisted of a ternary mixture of water, methanol, and acetonitrile (40:50:10 by volume); the flow rate was 1 mL min^{-1}. Further intermediates were determined by LC-MS/MS analysis. To identify reaction intermediates and to elucidate the mechanism of reaction pathways that control the photodegradation of 4-CP over different catalysts, diffuse reflectance FT-IR (Nicolet Nexus 470) was used to probe the absorption of 4-CP and intermediates to a catalyst surface. Chloride ions were performed by using an ion chromatograph (761 Compact IC, Metrohm). The eluent solution was 3.2 mM Na_2CO_3/1 mM $NaHCO_3$. Total organic carbon (TOC) was monitored with a Shimadzu TOC-5000 analyzer. Prior to injection into the TOC analyzer, the samples

10.1021/es801672a CCC: $40.75
Published on Web 10/22/2008

were filtrated with 0.45 μm Millipore filter to remove any particles. All experiments were carried out at least twice. The reported values are within the experimental error of ±3%.

Mott−Schottky Measurements. As-prepared samples for the fabrication of photoanode were obtained by mixing 1 mL of ethanol and 20 mg of as-prepared powder homogeneously. The as-prepared samples were spread on the indium−tin oxide (ITO) conducting glass (3 cm × 2 cm) with a sheet resistance of 15 Ω. After the films were dried under ambient conditions, they were sintered in air at 400 °C for 1 h. Mott−Schottky spectra were measured with a three-electrode cell, using the sintered fluorine doped $ZnWO_4$ photoanode as a working electrode, a platinum wire as the counter electrode, and a standard Ag/AgCl in saturated KCl as the reference electrode. The electrolyte was 0.1 M Na_2SO_4 (pH 7.2). Impedance spectra were obtained with a PARSTAT-2273 Advanced Electrochemical System (Princeton Applied Research) equipped with an impedance analyzer and controlled by a computer.

Photocatalytic Test. Photocatalytic activities of samples were evaluated by degradation of 4-CP under ultraviolet light irradiation of an 11 W low-pressure lamp with 254 nm. The average light intensity was 1.0 mW/cm^2. The radiant flux was measured with a power meter from the Institute of Electric Light Source (Beijing). 4-CP solutions (200 mL, 10 mg/L) containing 0.10 g of as-prepared samples without adjusting the pH value were placed in a glass beaker. The pH value of the dispersions was determined by the dissociation of 4-chlorophenol and hydroxylation of the catalyst surface before reaction and was 6.5 in our experiment. Before the light was turned on, the solution was first ultrasonicated for 10 min and then stirred for 10 min to ensure equilibrium between the catalysts. Volumes of 3 mL of sample solutions were taken at given time intervals and separated through centrifugation (4000 rpm, 10 min). Initial concentration of 4-CP solution was 10 mg/L, and its concentration variation was examined by a HPLC (Agilent 1100).

Results and Discussion

States of Fluorine in $ZnWO_4$ Crystals. Figure 1A shows XRD patterns of F-$ZnWO_4$ ($R_F = 0.4$) catalysts by annealing different times. All of the as-prepared samples can be matched with the XRD pattern of the pure $ZnWO_4$ [JCPDS code 15-0774] phase. The XRD patterns of F-$ZnWO_4$ ($R_F = 0.4$) catalysts with different annealing temperatures are similar, which demonstrates that annealing could not result in development of new crystal orientations but the crystallinity increases. However, a careful comparison of the (100) diffraction peaks in the range of 18−20° shows that the peak position of F-$ZnWO_4$ ($R_F = 0.4$) shifts slightly toward a higher 2θ value with the extension of annealing time (Figure 1B) and the increase of annealing temperature (Figure 1C). The same results are also presented in other diffraction peaks. Our previous research confirms that the observed shift toward a lower 2θ indicates interstitial doping with F^- ions (*4*). It is also found that the diffraction peak position of F-$ZnWO_4$ ($R_F = 0.4$) annealed at 450 °C for 4 h is similar to that of undoped $ZnWO_4$ (Figure 1B). Therefore, the upshift of diffraction peaks illustrated that interstitial fluorine can be eliminated with extension of annealing time. The influence of annealing temperature on crystal phase is shown in Figure 1C. The shift of 2θ value is smaller than that in Figure 1B. At 550 °C for 1 h, few fluorine ions exist in the interstitial lattice of $ZnWO_4$ comparison with doped $ZnWO_4$ ($R_F = 0.4$), indicating that the influence of the annealing time is more significant than that of the annealing temperature on the stability of the interstitial doping F^- ions.

Figure 2 shows an XPS survey spectrum of fluorine doped $ZnWO_4$ ($R_F = 0.4$) catalyst with different annealing times. It is clear that the as-prepared samples are mainly composed

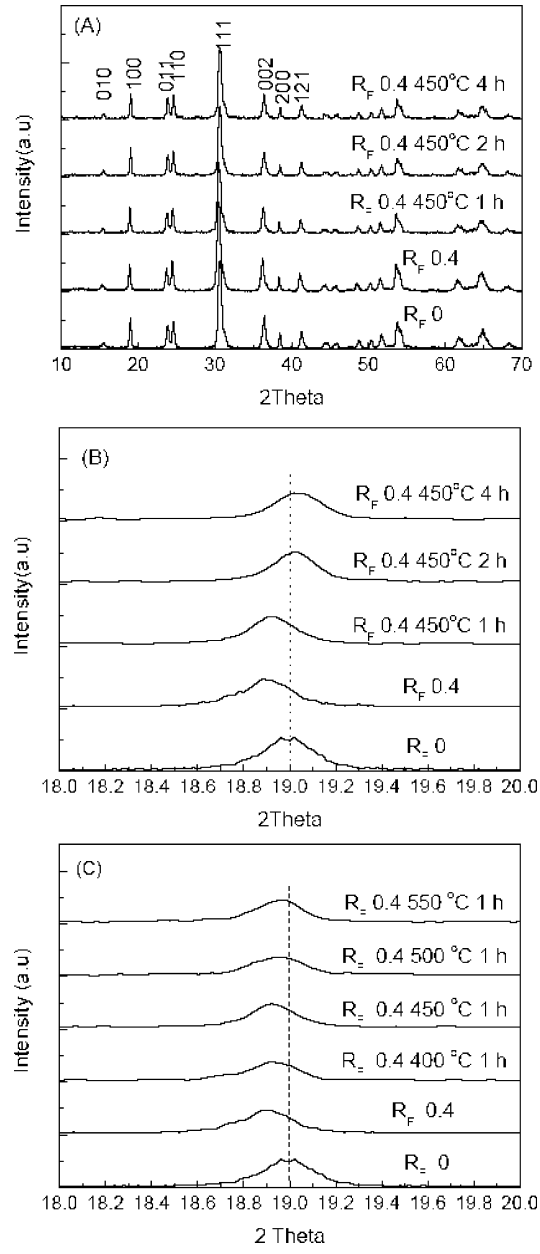

FIGURE 1. (A) XRD patterns of the samples prepared with different annealing times, (B) diffraction peak positions of the (100) plane in the range of 2θ = 18−20° with different annealing times, and (C) different annealing temperatures.

of Zn, W, O, and F elements and a trace amount of carbon. Quantitative analysis demonstrates that the atomic ratio of Zn/W/O/F is 1:1.2:5.4:0.07, when the F/Zn is 0.4 nominal atomic ratio. However, the atomic ratio of Zn/W/O/F is 1:1.3:5.6:0.01 after this sample was annealed at 450 °C for 2 h. An XPS spectrum of the F 1s peaks is shown in the inset of Figure 2. The binding energy of 684.1 eV corresponds to the fluorine ions in the interstitial lattice (*4*). The intensity of F 1s peak decreases when the sample $R_F = 0.4$ annealed at 450 °C for 2 h. On the basis of results of XRD, it can be concluded that fluorine ions exist in the interstitial lattice of the $ZnWO_4$ crystal and may be eliminated under the annealing conditions.

TEM photographs of F-$ZnWO_4$ ($R_F = 0.4$) catalysts annealed under different conditions are shown in Figure S1. The morphologies of as-prepared samples are homogeneous. It also can be seen that the particle sizes (~30 nm) are the same under different conditions. When annealing time is prolonged, the specific surface areas of as-prepared samples decrease from 24.8 ($R_F = 0.4$) to 21.1 m^2/g ($R_F = 0.4$ annealed

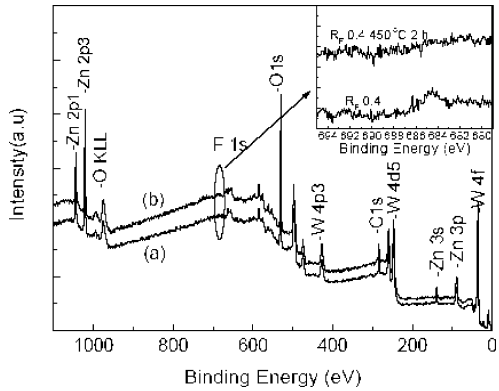

FIGURE 2. XPS survey spectrum of F-$ZnWO_4$ (R_F = 0.4) annealed different times (a) R_F = 0.4 and (b) R_F = 0.4 annealed at 450 °C for 2 h. The inset is the F 1s peak intensity of as-prepared samples.

at 450 °C for 4 h). The effects of annealing temperature are similar to that of annealing time. Therefore, the effects of annealing time and temperature are neglectable on morphologies, particle sizes, and specific surface areas.

The UV−visible diffuse reflectance spectra of as-prepared samples under different conditions are shown in Figure S2. The absorption optical of samples with different annealing temperatures are similar to the samples with different annealing times. The absorption spectra of the F^--doped $ZnWO_4$ samples show a stronger absorption in the UV range. It was due to doping with fluorine ions (*2, 4*). The samples with different annealing times present almost the same absorption edges which are red shift apparently. The band gap are estimated to be 3.26 and 3.60 eV for the samples with different annealing times and F-$ZnWO_4$ with R_F = 0.4, respectively (*4*).

Effects of Fluorine on Photocatalytic Activity of $ZnWO_4$. The effects of the initial 4-CP concentration on the photocatalytic rate are shown in Figure S3. It can be found that the initial concentration of 4-CP plays a significant role in the degradation rates. The photodegradation rate of F-$ZnWO_4$ for 4-CP is faster when initial concentration is lower. Therefore, the reaction of the photodegradation of 4-CP by as-prepared samples is apparent first-order kinetics of the Langmuir−Hinshelwood model, whose apparent relationships are due to the low concentration of 4-CP chosen. The 4-CP with initial concentration of 10 mg/L photodegradation over the as-prepared samples is shown in Figure 3. With an increase of annealing time, the photocatalytic activity of F-$ZnWO_4$ (R_F = 0.4) increases and reaches a maximum at 450 °C for 1 h and then decreases exceeding 1 h (Figure 3A). At 450 °C for 1 h, the photocatalyst reaches the highest photocatalytic activity which increases by 50% compared with that of F-$ZnWO_4$ without annealing. And 99% of 4-CP can be degraded in 180 min. However, with further increasing annealing time, the 4-CP removal efficiency decreases from 99.8% to 81.2%. In general, the high activity of photocatalyst was ascribed to the large surface area for absorbing substrate, small particle sizes to decrease the electron-hole migration distance, and high crystallinity to reduce electron-hole recombination rate (*12, 13*). On the basis of the results of XRD, BET, and TEM, the crystallinity of samples is fine, and specific surface areas and the particle sizes are almost the same after annealing treatment. Thus, the enhanced photoactivities may be assigned to the doping of fluorine ions, which results in an increase of the transfer-rate of photogenerated electrons to the photocatalyst surface (*4*). When the annealing time exceeds 1 h, few fluorine ions exist in the interstitial lattice of the $ZnWO_4$ crystal (Figures 1B and 2); therefore, the photocatalytic activities of as-prepared samples decrease despite a fine crystallinity. It is reasonable to believe

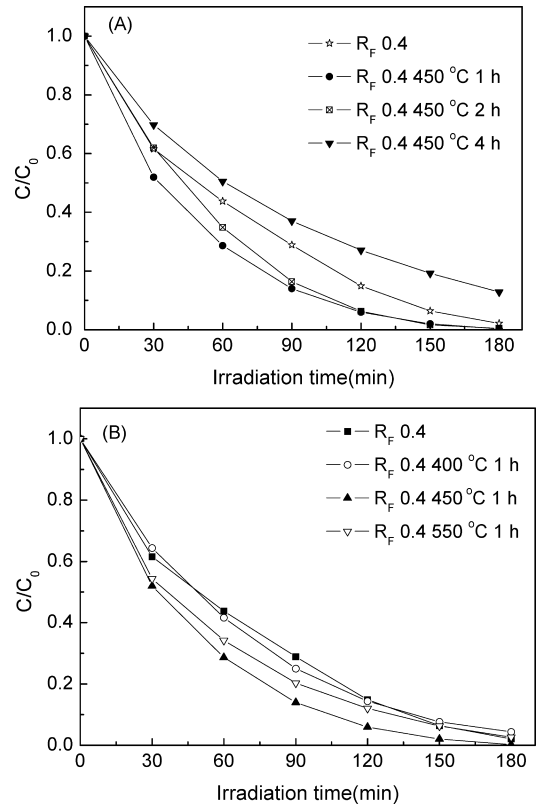

FIGURE 3. 4-CP photocatalytic degradation with initial concentration of 10 mg/L using different catalysts; catalyst loading: 0.5 g/L; pH = 6.5, λ = 254 nm. (A) R_F = 0.4 annealed at 450 °C for different times. (B) R_F = 0.4 annealed 1 h at different temperatures.

that the fluorine ions play a key role in enhancing photodegradation activity of 4-CP.

Figure 3B displays the relationship between the annealing temperature and photocatalytic activity. According to the trend of curve change, it can be seen that photocatalytic activity is slightly dependent on the annealing temperature. With an increasing of the annealing temperature, the photocatalytic activity of F-$ZnWO_4$ (R_F = 0.4) increases, reaches a maximum at 450 °C, and then decreases when the annealing temperature exceeds 450 °C. It also may be attributed to the fact that fewer fluorine ions are in the crystal lattices. Therefore, the photocatalytic activity of F-$ZnWO_4$ (R_F = 0.4) annealed at 550 °C decreases.

Effects of Fluorine on Intermediates of 4-CP. To evaluate the efficiency of catalytic systems and reveal some details of the reaction process, intermediates of 4-CP during the photocatalytic process were monitored by HPLC-MS-MS, and the results are displayed in Figure 4, Figure S4, and Table S1, respectively. HPLC graphs of 4-CP and of the intermediates after different irradiation times are shown in Figure S4. In the HPLC chromatogram, the peak *a* with retention time of 7.27 min is attributed to the initial 4-CP, and other peaks correspond to the intermediates. It can be seen that the peak *a* disappears quickly, the peak *b* attributed to 4-chlorocatechol (4-CC) increases and then decreases, and the other peaks slightly increase. The sample with R_F = 0.4 (in Figure S4A) presents similar results to those of annealed 450 °C for 2 h (in Figure S4B). The degradation pathway of 4-CP in our system does not change after annealing.

Detection and identification of intermediates produced in the degradation of 4-CP (initial concentration: 200 mg/L) were carried out by electrospray mass spectral techniques by both the positive-ions and negative-ion modes. The results are listed in Table S1 (Supporting Information). The initial

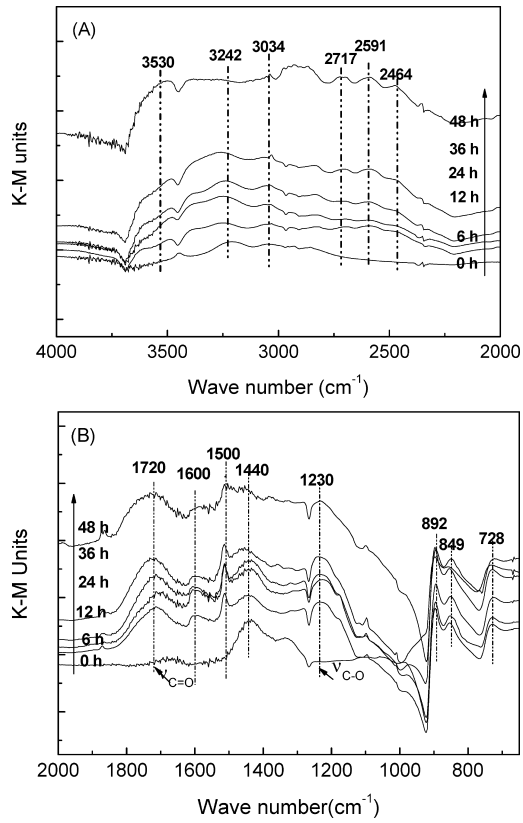

FIGURE 4. (A) Diffuse reflectance FT-IR spectroscopy of 4-CP absorbed on F-$ZnWO_4$ (R_F = 0.4) catalyst with different UV irradiation times and (B) a careful comparison in the range of 2000−650 cm^{-1}.

4-CP substrate is seen at $m/z = 127$ and 129 in the negative ion mode. Several intermediates are produced after 12 h of irradiation. The negative-ion mode signals at $m/z = 93$, 107, 109, 123, 125, and 143 are, respectively, those of phenol, benzoquinone (BQ), hydroquinone (HQ), hydroxybenzoquinone (HBQ), hydroxyhydroquinone (HHQ), and 4-chlorocatechol (4-CC). Bahnemann and co-workers (*14*) previously reported the generation of these intermediates in aqueous alkaline media (pH >7). Our current results show these substances to be formed in acidic media at pH < 7 (initial pH of 4-CP solution was 6.5), albeit under different experimental conditions. The above results maybe suggest different degradative mechanistic steps for F-$ZnWO_4$ photocatalytic degradation of 4-CP.

Diffuse reflectance FT-IR was used to follow the progress of the reaction over F-$ZnWO_4$ (R_F = 0.4) suspension with 4-CP. The annealed samples present similar results. In Figure 4A, differences between the IR spectra indicate that degradation of 4-CP due to photocatalytic reaction has occurred. The peak positions are noticed at 3530, 3242, 3043, 1660, 1440, 1320, and 728 cm^{-1}, indicating that 4-CP adsorbed on the catalyst surface (*10*). The peaks at 3530 and 3242 cm^{-1} are due to stretching vibrations of O−H, while the bands at 3043, 1660 cm^{-1} are the C=C stretching from the conjugated aryl. Peaks that represent O−H in-plane bending occur at 1320 and 1440 cm^{-1}. Bands at 728 cm^{-1} are originated from stretching vibrations of C−Cl. After irradiation of different times, there are pronounced changes in the spectra seen as a relative decrease or disappearances and significant shifts in many of the peaks. The growth in the height of the bands 2800−2500 cm^{-1} due to C−H stretching vibrations with the increasing of irradiation time indicates that an aldehydic structure is forming. However, aldehydes are not produced in intermediates of HPLC-MS-MS. The reason is that this compound appears after irradiation of 36 h, but several intermediates are produced after 12 h of irradiation. A careful comparison in the range of 2000−650 cm^{-1} is shown in Figure 4B. After 6 h, the bands due to C=O at 1720 cm^{-1} appear, and the strength of this peak increases with an increasing of irradiation time, indicating that quinonyl appears. HQ and BQ are the predominant intermediates that have been detected in our system of the photocatalytic degradation of 4-CP. This result is consistent with that in aqueous slurry studies of $PW_{12}O_{40}^{3-}$ photocatalytic degradation of 4-CP (*15*). The position of the O−H peak at 1440 cm^{-1} is identical to its position in a spectrum of 4-CP absorbed on catalyst. After 48 h this peak disappears, indicating that the 4-CP has been degraded to other intermediates. Bands at 1600, 1500, 892, 849, and 728 cm^{-1} are ascribed to 4-chlorocatechol adsorbed on a catalyst surface. The results of the diffuse reflectance FT-IR are in good agreement with that of the HPLC-MS -MS.

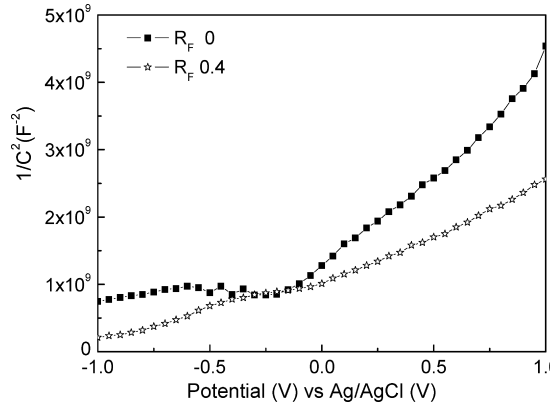

FIGURE 5. Mott−Schottky (MS) plots of the different catalysts film electrodes. The MS plots were obtained at a frequency of 1 kHz in an aqueous solution of Na_2SO_4 (0.1 M).

The temporal formation of Cl^- ions through dechlorination of 4-CP is illustrated in Figure S5. The annealing has an accelerating effect on the photocatalytic degradation and dechlorination of 4-CP. For $R_F = 0.4$ annealed at 450 °C for 2 h, the concentration of Cl^- rises to reach 96% (2.6 mg/L) of the theoretical quantity (2.7 mg/L) after 180 min of irradiation. This shows that few organic chlorine compounds exist in aqueous solution. However, the extent of dechlorination for $R_F = 0.4$ is about 64% after 180 min irradiation.

Effects of Fluorine on Electronic Properties of $ZnWO_4$. The transport of photogenerated electron through the n-type semiconductor to the collecting electrode is believed to occur by diffusion within extended states slowed by trapping/detrapping events (*16*). To understand the difference in electronic properties of the two $ZnWO_4$-based electrodes, Mott−Schottky (MS) measurements (Figure 5) were performed in the darkness by using the impedance technique (*17, 18*). A reversed sigmoidal plot was observed with an overall shape consistent with that typical for n-type semiconductors (*19*).

As we know from the classical Mott−Schottky theory, when the doping semiconductor space - charge region is depleted as it is under biasing conditions, the capacitance of space charge region can be described after simplification as

$$\frac{1}{C^2} = \left(\frac{2}{eN_d\epsilon_0\epsilon}\right)\left|V - V_{fb} - \frac{kT}{e}\right| \quad (1)$$

where e is the electronic charge (1.6×10^{-19} C), ϵ_0 is the permittivity of free space (8.86×10^{-12} F/m), ϵ is the dielectric constant (16.6 F/m) of the $ZnWO_4$ material, N_d is the dopant (donor or acceptor) concentration, k is the Boltzmann constant (1.38×10^{-23} J/K), T is the absolute temperature, V is the applied potential, and V_{fb} is the flat-band potential

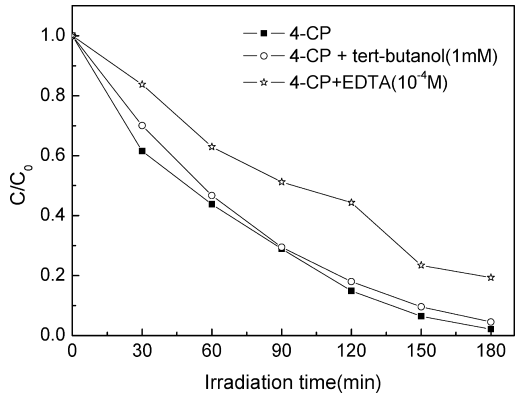

FIGURE 6. Effects of *tert*-butyl alcohol (TBA, 1 mM) and EDTA-Na (10^{-4} M) addition on photocatalytic degradation of 4-CP in solutions of F-$ZnWO_4$ (R_F = 0.4).

(*20*). It shows that when $1/C^2$ is zero, the *x*-intercept is equal to the flat band potential V_{fb}, and the dopant density N_d can be determined from the slope of the linear region.

Based on Figure 5, the flat-band potential of both samples is obtained. The calculated V_{fb} for undoped and doped $ZnWO_4$ (R_F = 0.4) electrodes are −0.40 and −0.67 V versus Ag/AgCl (in saturated KCl), respectively. The V_{fb} of $ZnWO_4$ films at the pH 6.0 electrolyte was reported to be approximately −0.36 V versus SCE (*21*). The almost agreeable results are obtained in this research system. The V_{fb} of the doped $ZnWO_4$ shows a large negative shift of the conduction band as compared with the undoped $ZnWO_4$. In some case, the presence of a large number of surface states or oxygen vacancies can result in a considerable change of band position (*20*). In addition, the slope of the linear region for the doped sample shows a much lower value, clearly indicating significantly higher donor density for the doped electrode. According to photocatalytic mechanism (*22*), the higher donor density for the doped electrode, the photocatalytic degradation rate is faster. This is further proved that the photocurrent of doped sample is larger than that of undoped sample (*4*). Therefore, the enhancement of photocatalytic activity could be attributed to the higher separation efficiency of electron-hole pairs, and a large number of holes participated in the photocatalytic process caused by fluorine.

Photocatalytic Mechanism. In most of the proposed mechanisms of the photocatalytic degradation of organic pollutants mediated by semiconductors, the highly oxidizing (surface-bound) hydroxyl radical, which originates from the oxidation of chemisorbed OH^- or H_2O by photogenerated valence band holes, is regarded as the main oxidative species responsible for the degradation (*7*−*9, 23*). No doubt some reactions can also be initiated by direct hole oxidation, especially when the adsorption by the substrates is rather extensive and the concentrations of substrates are relatively high (*15, 24, 25*). To verify the role of OH radicals, the 4-CP/F-$ZnWO_4$ system was examined by DMPO spin-trapped ESR spectroscopy to monitor the active radicals during the photocatalytic reaction process. The results are shown in Figure S6. No signals are observed either when the 4-CP/F-$ZnWO_4$ suspension is preformed in the dark or under UV light. The photodegradation of 4-CP on R_F = 0.4 was compared in the absence or presence of *tert*-butyl alcohol (TBA), a widely used OH radicals scavenger (Figure 6) (*26*). The addition of TBA slightly affected the photocatalytic degradation rate of 4-CP under UV irradiation. This indicates that the photocatalytic degradation process should not be mediated by OH radicals, which is different from the photocatalytic process of 4-CP in Ti-based suspension (*6*−*9*). On the contrary, the photocatalytic activity of F-$ZnWO_4$ (R_F = 0.4) could be moderately inhibited by the addition of capture for holes (EDTA-Na), indicating that holes are the main active oxygen species involved in the photoreaction catalyzed process. As a result, fewer •OH radicals are involved in the degradation of 4-CP on fluorine doped $ZnWO_4$ (R_F = 0.4). The direct hole transfers mainly govern the photocatalytic process, which is consistent with the literature (*24, 25*).

In the current work, ESR measurements and active species trapped experiment for the first time give direct evidence that the active species (•OH and O_2•$^-$) are irresponsible for the photodecomposition of 4-CP, strongly suggesting that the photocatalytic reaction of organic compounds in the powdered F-$ZnWO_4$ system may proceed via direct reactions with holes trapped. F-doped $ZnWO_4$ absorb UV light to generated electron-hole pairs (reaction 2). Valence band holes (h_{vb}^+) are powerful reactive species, which attack at the C−Cl carbon position leading to formation of HQ and to dechlorination of chemisorbed 4-CP (reaction 3). Note photodegradation of 4-CP by •OH on the sample surface, though not precluded by our present date.

$$\text{F-ZnWO}_4 + h\nu \rightarrow \text{F-ZnWO}_4(e_{cb} + h_{vb}) \quad (2)$$

$$h_{vb}^+ + \text{4-CP} \rightarrow \text{dechlorinated intermediates and products} \rightarrow \text{CO}_2 + \text{H}_2\text{O} + \text{Cl}^- \quad (3)$$

The loss of total organic carbon (TOC) on irradiation is illustrated in Figure S7. The reduction rate of TOC reduction is slower than that of the degradation of the 4-CP; 60% of TOC still remains in the suspension after 180 min of irradiation. The slow mineralization seems to be due to the aromatic intermediates concentrations remaining unchanged (*15, 27*).The decay of TOC could be divided into two stages: the first stage was the lag phase, where the TOC reduction was insignificant because the dominant reaction was the 4-CP to aromatic intermediates. The lag phase was followed by a mild TOC decay, in which 70% of the 4-CP was degraded, and the high molecular weight intermediates were degraded to a lower one. Finally, the TOC was removed completely with increasing the irradiation time.

The stability of the photocatalyst was also studied. The results are shown in Figure S8. After photodegradation of 4-CP, the crystal structure of the photocatalyst is not changed, indicating that the sample is fairly stable during the photodegradative process.

The photocatalytic activity of F-$ZnWO_4$ can be further enhanced by annealing. The fluorine ions play a key role in enhancing photodegradation activity of 4-CP. The enhancement of photocatalytic activity could be attributed to the higher separation efficiency of electron-hole pairs, and a large number of holes participated in the photocatalytic process caused by fluorine. The photodegradation of 4-CP in the powdered F-doped $ZnWO_4$ system proceeds via direct reactions with holes trapped.

Acknowledgments

This work was partly supported by Chinese National Science Foundation (20433010 and 20571047), National Basic Research Program of China (2007CB613303), and SRFDP (2006003082).

Supporting Information Available

TEM, UV-DRS, influence of initial concentration on photodegradation of 4-CP, HPLC of intermediates of 4-CP, changes of concentration of Cl^-, ESR, TOC, XRD of F-$ZnWO_4$ annealed 450 °C 2 h after irradiation and MS-MS, Figures S1−S8, and Table S1. This material is available free of charge via the Internet at http://pubs.acs.org.

Literature Cited

(1) Hattori, A.; Tada, H. High photocatalytic activity of F-doped TiO_2 film on glass. *J. Sol-Gel Sci. Technol.* **2001**, *22*, 47–52.

(2) Yu, J. C.; Yu, J. G.; Ho, W.; Jiang, Z.; Zhang, L. Effects of F-doping on the photocatalytic activity and microstructures of nanocrystalline TiO_2 powders. *Chem. Mater.* **2002**, *14*, 3808–3816.
(3) Wang, J. S.; Yin, S.; Zhang, Q. W.; Saito, F.; Sato, T. Mechanochemical synthesis of $SrTiO_{3-x}F_x$ with high visible light photocatalytic activities for nitrogen monoxide destruction. *J. Mater. Chem.* **2003**, *13*, 2348–2352.
(4) Huang, G. L.; Zhu, Y. F. Enhanced photocatalytic activity of $ZnWO_4$ catalyst via fluorine doping. *J. Phys. Chem. C* **2007**, *111*, 11952–11958.
(5) Yue, B.; Zhou, Y.; Xu, J. Y.; Wu, Z. Z.; Zhang, X.; Zou, Y. F.; Jin, S. L. Photocatalytic degradation of aqueous 4-chlorophenol by silica-immobilized polyoxometalates. *Environ. Sci. Technol.* **2002**, *36*, 1325–1329.
(6) Zhang, X. W.; Zhou, M. H.; Lei, L. C. Preparation of an Ag-TiO_2 photocatalyst coated on activated carbon by MOCVD. *Mater. Chem. Phys.* **2005**, *91*, 73–79.
(7) Moonsiri, M.; Rangsunvigit, P.; Chavadej, S.; Gulari, E. Effects of Pt and Ag on the photocatalytic degradation of 4-chlorophenol and its by-products. *Chem. Eng. J.* **2004**, *97*, 241–248.
(8) Kim, S.; Choi, W. Visible-light-induced photocatalytic degradation of 4-Chlorophenol and phenolic compounds in aqueous suspension of pure titania: demonstration the existence of a surface-complex-mediated path. *J. Phys. Chem. B* **2005**, *109*, 5143–5149.
(9) Horikoshi, S.; Tokunaga, A.; Watanabe, N.; Hidaka, H.; Serpone, N. Environmental remediation by an integrated microwave/UV illumination technique - IX. Peculiar hydrolytic and co-catalytic effects of platinum on the TiO_2 photocatalyzed degradation of the 4-chlorophenol toxin in a microwave radiation field. *J. Photochem. Photobiol. A: Chem.* **2006**, *177*, 129–143.
(10) Stafford, U.; Gray, K, A.; Kamat, P, V.; Varma, A. An in situ diffuse reflectance FTIR investigation of photocatalytic degradation of 4-chlorophenol on a TiO_2 powder surface. *Chem. Phys. Lett.* **1993**, *205*, 55–61.
(11) Jiang, D. L.; Zhang, S. Q.; Zhao, H. J. Photocatalytic degradation characteristics of different organic compounds at TiO_2 nanoporous film electrodes with mixed anatase/rutile phases. *Environ. Sci. Technol.* **2007**, *41*, 303–308.
(12) Li, D.; Haneda, H. Morphologies of zinc oxide particles and their effects on photocatalysis. *Chemosphere* **2003**, *51*, 129–137.
(13) Ohno, T.; Tokieda, K.; Higashida, S.; Matsumura, M. Synergism between rutile and anatase TiO_2 particles in photocatalytic oxidation of naphthalene. *Appl. Catal. A: Chem.* **2003**, *244*, 383–391.
(14) Theurich, J.; Lindner, M.; Bahnemann, W, D. Photocatalytic degradation of 4-chlorophenol in aerated aqueous titanium dioxide suspensions: a kinetic and mechanistic study. *Langmuir* **1996**, *12*, 6368–6376.
(15) Kim, S.; Park, H.; Choi, W. Comparative study of homogeneous and heterogeneous photocatalytic redox reactions: $PW_{12}O_{40}^{3-}$ vs TiO_2. *J. Phys. Chem. B* **2004**, *108*, 6402–6411.
(16) Zaban, A.; Meier, A.; Gregg, B. A. Electric potential distribution and short-range screening in nanoporous TiO_2 electrodes. *J. Phys. Chem. B* **1997**, *101*, 7985–7990.
(17) Tse, K. Y.; Nichols, B. M.; Yang, W. S.; Butler, J. E.; Russell, J. N.; Hamers, R. J. Electrical properties of diamond surfaces functionalized with molecular monolayers. *J. Phys. Chem. B* **2005**, *109*, 8523–8532.
(18) Fabregat-Santiago, F.; Garcia-Belmonte, G.; Bisquert, J.; Bogdanoff, P.; Zaban, A. Mott-Schottky analysis of nanoporous semiconductor electrodes in dielectric state deposited on SnO_2 (F) conducting substrates. *J. Electrochem. Soc.* **2003**, *150*, 293–298.
(19) Park, S. M.; Yoo, J. S. Electrochemical impedance spectroscopy for better electrochemical measurements. *Anal. Chem.* **2003**, *75*, 455–461.
(20) Wang, G.; Wang, Q.; Lu, W.; Li, J. Photoelectrochemical study on charge transfer properties of TiO_2-B nanowires with an application as humidity sensors. *J. Phys. Chem. B* **2006**, *110*, 22029–22034.
(21) Zhao, X.; Yao, W. Q.; Wu, Y.; Zhang, S. C.; Yang, H. P.; Zhu, Y. F. Fabrication and photoelectrochemical properties of porous $ZnWO_4$ film. *J. Solid. State Chem.* **2006**, *179*, 2562–2570.
(22) Maeda, H.; Ikeda, K.; Hashimoto, K.; Ajito, K.; Morita, M.; Fujishima, A. Microscopic observation of TiO_2 photocatalysis using scanning electrochemical microscopy. *J. Phys. Chem. B* **1999**, *103*, 3213–3217.
(23) Hoffmann, M. R.; Martin, S. T.; Choi, W. Environmental applications of semiconductor photocatalysis. *Chem. Rev.* **1995**, *95*, 69–96.
(24) Zhu, S.; Xu, T.; Fu, H.; Zhao, J.; Zhu, Y. Synergetic effect of Bi_2WO_6 photocatalyst with C_{60} and enhanced photoactivity under visible irradiation. *Environ. Sci. Technol.* **2007**, *41*, 6234–6239.
(25) Fu, H. B.; Pan, C. S.; Yao, W. Q.; Zhu, Y. F. Visible-light-induced degradation of rhodamine B by nanosized Bi_2WO_6. *J. Phys. Chem. B* **2005**, *109*, 22432–22439.
(26) Minero, C.; Mariella, G. ; Maurino, V.; Vione, D.; Pelizzetti, E. Photocatalytic transformation of organic compounds in the presence of inorganic ions. 2. Competitive reactions of phenol and alcohols on a titanium dioxide-fluoride system. *Langmuir* **2000**, *16*, 8964–8972.
(27) Mylonas, A; Hiskia, A.; Papaconstantinou, E. Contribution to water purification using polyoxometalates. Aromatic derivatives, chloroacetic acids. *J. Mol. Catal. A: Chem.* **1996**, *114*, 191–200.

ES801672A